

Preliminary study on image reconstruction for limited-angular-range dual-energy CT using two-orthogonal, overlapping arcs

Buxin Chen¹, Zheng Zhang¹, Dan Xia¹, Emil Y. Sidky¹, and Xiaochuan Pan^{1,2}

¹Department of Radiology, The University of Chicago, Chicago, IL, USA

²Department of Radiation and Cellular Oncology, The University of Chicago, Chicago, IL, USA

ABSTRACT

Dual-energy CT (DECT) of limited-angular ranges (LARs) collects data from angular ranges smaller than π for low- and high-kVp scans, and thus may potentially be exploited for reducing scanning time and radiation dose and for avoiding collision between the imaged object and the moving gantry of the scanner. Image artifacts resulting from beam hardening (BH) and limited-angular range (LAR) can be suppressed by using the data-domain decomposition and the directional-total-variation (DTV) algorithm for image reconstruction. In this work, we investigate two-orthogonal-arc (TOA) scanning configuration with overlapping arcs for collecting LAR DECT data, in an effort to reduce LAR artifacts and improve quantitative accuracy of estimated physical quantities. The TOA configuration consists of two arcs, of equal LAR, whose centers are positioned 90° apart, and is designed to reduce the ill-conditionedness of the imaging system matrix. The data are decomposed into basis sinograms, from which basis images are reconstructed using the DTV algorithm. Visual inspection of the monochromatic images and quantitative estimation of the effective atomic numbers suggest that the TOA configuration, as compared to the single-arc (SA) configuration of the same total angular range, can help reduce remaining LAR artifacts and bias in the estimated atomic number relative to the reference values from the full-angular-range data of 360° .

1. INTRODUCTION

Current dual-energy CT (DECT) typically collect data, of either low- or high-kVp spectrum, in a full-scan, or at least short-scan, rotation.^{1,2} Images are then reconstructed often by use of conventional algorithms, such as FBP, from kVp sinogram directly or decomposed basis sinogram. One-step algorithms have also been investigated for reconstructing basis images directly from full-scan data.³ DECT of limited-angular ranges (LARs)^{4,5} collects data from angular ranges smaller than π for low- and high-kVp scans, and thus may be potentially useful for reducing scanning time and radiation dose and for avoiding collision between the imaged object and the moving gantry of the scanner. In LAR DECT, LAR artifacts in images are usually more dominant than other ones, such as beam hardening (BH), and are thus subject to more focus and effort in artifacts correction.^{6,7} Simultaneous correction of LAR and BH artifacts may help reduce image artifacts and improve quantitative accuracy in LAR DECT, especially for extremely small angular ranges. In this work, we aim to improve simultaneous correction for LAR and BH artifacts, and thus quantitative reconstruction accuracy, by investigating the two-orthogonal-arc (TOA) configuration for DECT with overlapping rays, which can help alleviate the ill-conditionedness in the system matrix.

Numerical studies are carried out with a suitcase phantom containing different materials. LAR scanning configurations are set up with overlapping rays from low- and high-kVp scans, i.e., the scanning arcs of the low- and high-kVp scans are identical. For either kVp scan, the scanning arcs consist of two LAR arcs, whose centers are separated by 90° . Data are first decomposed into basis sinograms, and basis images are then reconstructed by use of the directional-total-variation (DTV) algorithm. This primal-dual algorithm has been developed for solving a DTV-constrained, data- ℓ_2 -minimization problem.^{4,6} Basis images are combined into monochromatic images for visual assessment, and then used for computing effective atomic numbers of different materials in the phantom. Results are compared with those from the single-arc (SA) configuration with the same total angular ranges.

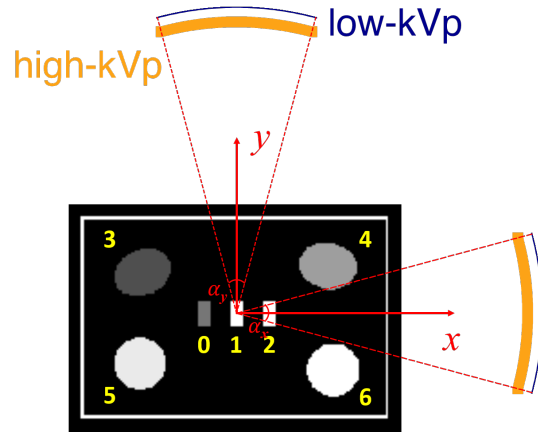


Figure 1: The TOA scanning configuration with overlapping LAR arcs of low- and high-kVp spectra, for collecting dual-energy data from a suitcase phantom, containing different materials including C, Al, Ca, water, ANFO, teflon, and PVC, shown as ROIs 0-6 respectively.

2. MATERIALS AND METHODS

2.1 Two-orthogonal-arc configuration

A 2D circular fan-beam geometry is considered, as shown in Fig. 1, while the approach can readily be extended to non-circular fan-beam geometry and to circular/non-circular 3D cone-beam geometry. The source-to-rotation and source-to-detector distances are 100 cm and 150 cm, respectively, while the linear detector is 32 cm in length with 512 bins. The scanning arcs of low- and high-kVp spectra are identical, thus generating overlapping rays suitable for data-domain decomposition. With the TOA configuration, for each of the low- and high-kVp scan, there are two scanning arcs, separated by 90° from center to center, covering LARs of α_x and α_y (it is assumed that the two arcs are symmetric relative to the x and y axes in the image array, respectively). Given a total angular range $\alpha_\tau = \alpha_x + \alpha_y$, there are many different ways of distributing between α_x and α_y . In this work, we focus on the case with equal range, $\alpha_\tau/2$, i.e., $\alpha_x = \alpha_y = \alpha_\tau/2$, because studies have suggested that TOA with equal-range arcs might perform better than other distributions.⁸ Data are also collected using a SA configuration with $\alpha_y = \alpha_\tau$ and $\alpha_x = 0$. A set of total angular ranges is studied with $14^\circ \leq \alpha_\tau \leq 180^\circ$, with a fixed angular interval of 0.25° per view. In this study, we focus on the three smallest LARs of $\alpha_\tau = 20^\circ$, and 30° , which are the most challenging. The TOA configuration for LAR DECT can be readily implemented with existing DECT technologies, such as dual-source DECT, sandwiched detector, fast-kVp-switching X-ray tubes, and also sequential scans.

2.2 Dual-energy data

A digital suitcase phantom is used containing different materials that are challenging to be differentiated and identified with conventional CT, including circular and elliptical ROIs filled with water, ammonium nitrate and fuel oil (ANFO), teflon, and PVC, as well as three bar-shaped ROIs of single-element materials, C, Al, and Ca. The discrete phantom is set up on an 175×256 image array with 0.7-mm square pixels, while each pixel is labeled with a material type and thus associated with the material's linear attenuation coefficients from the NIST database. Dual-energy data are generated using a non-linear data model incorporating the spectral integral, such as Eq. (1) in Ref.,⁶ with simulated low- and high-kVp spectra at 80 kVp and 140 kVp using the TASMIC model.⁹ Both noiseless and noisy data are generated, with Poisson noise added to the noiseless data, corresponding to 4.5×10^5 and 6.75×10^5 noise equivalent quanta (NEQ) per ray in the air scan for $\alpha_\tau = 30^\circ$ and 20° , respectively, such that the total NEQ is constant for different LARs.

Once data, namely, low- and high-kVp sinograms, are generated, they are decomposed into basis sinograms for BH correction using a well recognized data-domain decomposition method.¹⁰ An interaction-based basis

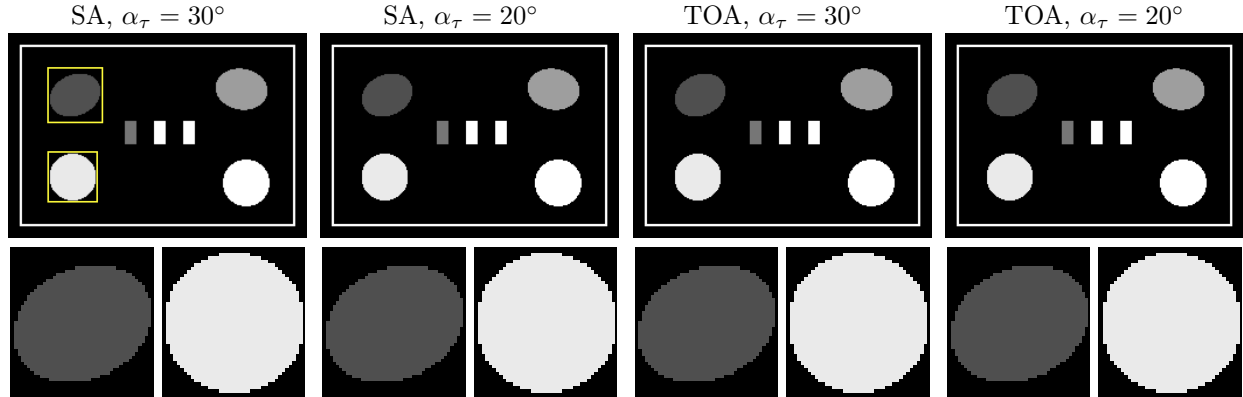


Figure 2: Monochromatic images (top row) of the suitcase phantom at 40 keV obtained from noiseless data over SAs (columns 1 & 2) of $\alpha_\tau = 30^\circ$ and 20° , and TOAs (columns 3 & 4) of the same total angular range by use of the DTV algorithm, along with their respective zoomed-in views (bottom row). The zoomed-in regions are enclosed by the rectangular boxes including ROIs 3 and 5, as depicted in the top-left image. Display window: $[0.1, 0.65] \text{ cm}^{-1}$.

decomposition is used, where photoelectric effect (PE) and Compton scattering (KN) are the two bases with $1/E^3$ and the Klein-Nishina formula as their spectral responses. The low- and high-kVp spectra are assumed to be known exactly, therefore minimizing the impact of spectrum mismatch in BH correction.

2.3 Image reconstruction

With decomposed basis sinogram, \mathbf{l}_{PE} and \mathbf{l}_{KN} for photoelectric effect and Compton scattering, the reconstructions of basis images, \mathbf{b}_{PE} and \mathbf{b}_{KN} , can be formulated into two separate convex optimization problems as

$$\begin{aligned} \mathbf{b}_k^* &= \underset{\mathbf{b}_k}{\operatorname{argmin}} \frac{1}{2} \|\mathbf{l}_k - \mathcal{A} \mathbf{b}_k\|_2^2 \\ \text{s.t. } &\|\mathcal{D}_x \mathbf{b}_k\|_1 \leq t_{kx}, \quad \|\mathcal{D}_y \mathbf{b}_k\|_1 \leq t_{ky}, \end{aligned} \quad (1)$$

where $k = \text{PE}$ or KN ; \mathcal{A} is the discrete X-ray transform (DXT) of the TOA configuration; and $\|\mathcal{D}_x \mathbf{b}_k\|_1$ and $\|\mathcal{D}_y \mathbf{b}_k\|_1$ are ℓ_1 norms of the image partial derivatives along the x and y axes, respectively, also referred to as the image's DTVs. The separate DTV constraints along the image array's orthogonal directions have been shown to reduce effectively the directional artifacts in CT images reconstructed from LAR data. The two convex optimization problems in Eq. (1) for the two bases are solved by the DTV algorithm,⁴ which is based on a general primal-dual algorithm.¹¹

2.4 Evaluation

From basis images reconstructed, monochromatic images are formed as a linear combination of basis images and visually assessed for artifact reduction. Further, the effective atomic number, z , can be estimated from the interaction-based basis images, due to different orders of z -dependence for the photoelectric effect and Compton scattering interactions.^{1,12} In particular, a linear relationship in the log-log domain can be assumed between z and the ratio of the basis image values, where the slope and intercept can be fitted using the single-element materials in the phantom with known z values.

3. RESULTS

We show in Fig. 2 monochromatic images at 40 keV from noiseless LAR data collected over SAs of $\alpha_\tau = 20^\circ$ and 30° , and over TOAs of equal total angular ranges. No visual LAR artifacts can be observed in the images. Quantitatively, the monochromatic images from the TOA scan are closer to the reference image from full-scan range data of 360° than those from the SA scan in terms of the normalized root-mean-square-error (nRMSE)

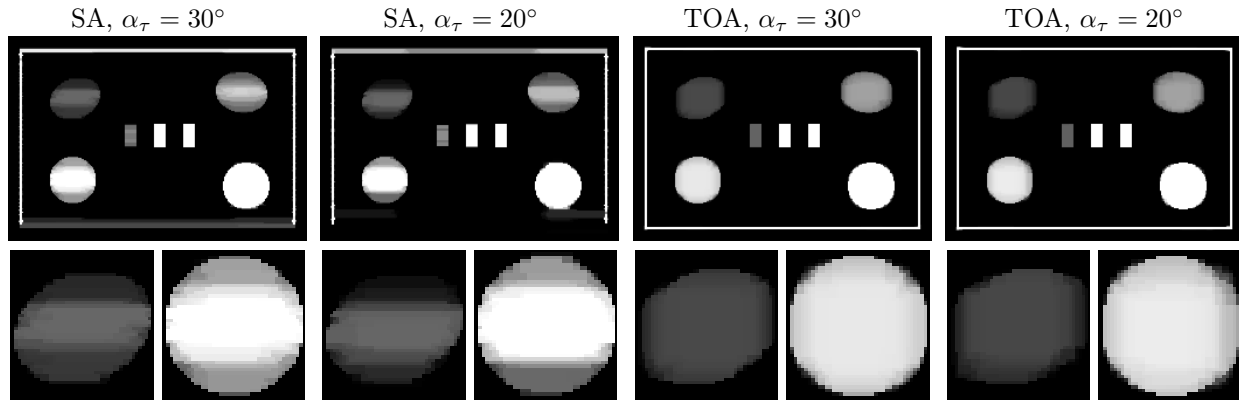


Figure 3: Monochromatic images (top row) of the suitcase phantom at 40 keV obtained from noisy data over SAs (columns 1 & 2) of $\alpha_\tau = 30^\circ$ and 20° , and TOAs (columns 3 & 4) of the same total angular range by use of the DTV algorithm, along with their respective zoomed-in views (bottom row). The zoomed-in regions are enclosed by the rectangular boxes including ROIs 3 and 5, as depicted in the top-left image in Fig. 2. Display window: $[0.1, 0.65] \text{ cm}^{-1}$.

Table 1: Estimated atomic number of ROI 3 (water) from noiseless and noisy data collected over SA and TOA of the same total angular coverage of 30° and 20° . The reference value from full-scan 360° noiseless data is 7.49.

		$\alpha_\tau = 30^\circ$	$\alpha_\tau = 20^\circ$
noiseless	SA	7.49	7.49
	TOA	7.49	7.49
noisy	SA	7.97	7.36
	TOA	7.50	7.38

(nRMSE = 4.88×10^{-5} and 1.05×10^{-4} for 30° and 20° over SA, respectively, and 5.29×10^{-6} and 6.76×10^{-6} over TOA.)

We show the same results with noisy data in Fig. 3. Horizontal shading artifacts can be observed in the images from data collected over SAs of the extremely small LARs under investigation. The circular and elliptical disks are distorted, and the horizontal edges of the suitcases are difficult to recover, since they are mostly parallel to the SAs and are characterized as “invisible boundaries”.¹³ In images from data collected over TOAs, there is no significant shape distortion to the circular and elliptical disks, while the edges of the suitcase are recovered.

From basis images of PE and KN, we can estimate the effective atomic numbers by assuming a linear relationship in the log-log domain between z and the ratio of the basis image values. The coefficients can be calibrated using single-element materials with known z number, such as C, Al, and Ca in the phantom. We show in Tables 1 and 2 the estimated z numbers of ROIs 3 (water) and 5 (teflon), respectively, from both noiseless and noisy data over SAs and TOAs. The reference values, 7.49 and 8.50, are calculated from the noiseless data collected over the full-scan range of 360° . It can be observed that the TOA configuration can help reduce the bias in the quantitative estimation of effective atomic number, relative to the reference values, as compared to the SA configuration.

Table 2: Estimated atomic number of ROI 5 (teflon) from noiseless and noisy data collected over SA and TOA of the same total angular coverage of 30° and 20° . The reference value from full-scan 360° noiseless data is 8.50.

		$\alpha_\tau = 30^\circ$	$\alpha_\tau = 20^\circ$
noiseless	SA	8.50	8.50
	TOA	8.50	8.48
noisy	SA	9.31	9.04
	TOA	8.46	8.48

4. CONCLUSION

In this work, we have proposed and investigated the two-orthogonal-arc scanning configuration with overlapping arcs, in combination with the DTV algorithm, for improving artifact correction and quantitative accuracy in DECT with LAR data. Numerical studies were carried out with a digital suitcase phantom, from which dual-energy data, with both SA and TOA configurations of the same total angular range, were generated using a non-linear data model. With overlapping arcs of low- and high-kVp scans, the kVp sinograms were decomposed into interaction-based basis sinograms by use of a data-domain decomposition method for BH correction. Basis images were then reconstructed from the basis sinograms by use of the DTV algorithm. Monochromatic images at 40 keV were combined for visual inspection and effective atomic numbers were estimated. Results suggest that the TOA configuration, as compared to the SA configuration of the same total angular range as low as 20° , can effectively reduce the remaining artifacts in monochromatic images obtained with the DTV algorithm, and also yield accurate estimation of effective atomic numbers relative to the reference values from the full-angular-range data of 360° . Further investigation will focus on adding other physical factors, such as scatter, and using phantoms with different anatomies and structures.

ACKNOWLEDGMENT

This work was supported in part by NIH Grants Nos. R01-EB026282, R01-EB023968, and 1R21-CA263660-01A1. The contents of this article are solely the responsibility of the authors and do not necessarily represent the official views of the National Institutes of Health.

REFERENCES

- [1] R. E. Alvarez and A. Macovski, "Energy-selective reconstructions in X-ray computerised tomography," *Phys. Med. Biol.*, vol. 21, no. 5, pp. 733–744, 1976.
- [2] T. G. Flohr, C. H. McCollough, H. Bruder, M. Petersilka, K. Gruber, C. Süß, M. Grasruck, K. Stierstorfer, B. Krauss, R. Raupach *et al.*, "First performance evaluation of a dual-source CT (DSCT) system," *Eur. Radiol.*, vol. 16, no. 2, pp. 256–268, 2006.
- [3] B. Chen, Z. Zhang, D. Xia, E. Y. Sidky, and X. Pan, "Non-convex primal-dual algorithm for image reconstruction in spectral CT," *Comput. Med. Imaging Graph.*, vol. 87, p. 101821, 2021.
- [4] Z. Zhang, B. Chen, D. Xia, E. Y. Sidky, and X. Pan, "Directional-TV algorithm for image reconstruction from limited-angular-range data," *Med. Image Anal.*, vol. 70, p. 102030, 2021.
- [5] H. Zhang and Y. Xing, "Reconstruction of limited-angle dual-energy CT using mutual learning and cross-estimation (mlce)," in *Proc. SPIE Med. Imag.: Phys. Med. Imag.*, vol. 9783. International Society for Optics and Photonics, 2016, p. 978344.
- [6] B. Chen, Z. Zhang, D. Xia, E. Y. Sidky, and X. Pan, "Dual-energy ct imaging with limited-angular-range data," *Phys. Med. Biol.*, vol. 66, no. 18, p. 185020, 2021.
- [7] —, "Dual-energy ct imaging over non-overlapping, orthogonal arcs of limited-angular ranges," *Journal of X-ray Science and Technology*, no. Preprint, pp. 1–11, 2021.
- [8] Z. Zhang, B. Chen, D. Xia, E. Y. Sidky, and X. Pan, "Image reconstruction from data over two orthogonal arcs of limited-angular ranges," *Med. Phys.*, vol. preprint, pp. 1–13, 2022.
- [9] A. M. Hernandez and J. M. Boone, "Tungsten anode spectral model using interpolating cubic splines: Unfiltered X-ray spectra from 20 kv to 640 kv," *Med. Phys.*, vol. 41, no. 4, p. 042101, 2014.
- [10] Y. Zou and M. D. Silver, "Analysis of fast kv-switching in dual energy CT using a pre-reconstruction decomposition technique," in *Proc. SPIE Med. Imag.: Phys. Med. Imag.*, vol. 6913, 2008, p. 691313.
- [11] E. Y. Sidky, J. H. Jorgensen, and X. Pan, "Convex optimization problem prototyping for image reconstruction in computed tomography with the Chambolle-Pock algorithm," *Phys. Med. Biol.*, vol. 57, no. 10, pp. 3065–3091, 2012.
- [12] Z. Ying, R. Naidu, and C. R. Crawford, "Dual energy computed tomography for explosive detection," *J. X-Ray Sci. Technol.*, vol. 14, no. 4, pp. 235–256, 2006.
- [13] E. T. Quinto, "Artifacts and visible singularities in limited data X-ray tomography," *Sens. Imaging*, vol. 18, no. 1, p. 9, 2017.